EFFECT OF CRYSTALLINE MORPHOLOGY ON HEAT TRANSFER THROUGH MOULD FLUX

Miyuki Hayashi, Kazuki Matsuo & Kazuhiro Nagata
Tokyo Institute of Technology, Japan

Hideko Nakada
The University of Tokyo, Japan

ABSTRACT

Our previous research has revealed that in the mould fluxes for medium carbon steel, the reflectivity of the crystalline slag layer formed in mould flux film is an efficient factor for further reducing the heat flux in the film. The radiation is reflected at the interface between the liquid (slag) and the crystalline layers and/or at the crystal grain boundaries, resulting in the reduction in the total heat flux across the flux film, leading to mild cooling. In order to investigate the mechanism of the reflection of radiation by the crystalline slag layer, the dependencies of the heat flux on the thickness of the crystalline layers and the roughness of the interface between the slag and the crystalline layers have been investigated. The heat flux is independent of the thicknesses of the crystalline, cubic-crystal, dendrite and slag layers, which indicates that the reflection of radiation at the crystal grain boundaries does not affect the total heat flux across the sample. The flux film having the larger width of the dendrite at the interface between the slag and the crystalline layers exhibits the smaller heat flux. This result implies that the reflection of radiation at the interface between the liquid and the crystalline slag layers is a dominant factor for reducing the heat flux across the flux film.

INTRODUCTION

In the continuous casting of steel, the mould flux, which mainly consists of $CaO\text{-}SiO_2\text{-}CaF_2$ system, has two main functions: i) lubrication between the solidified steel shell and the water-cooled copper mould and ii) control of the heat transfer from the steel shell to the mould. The heat flux profoundly affects the surface quality of steel especially at the initial stage of the solidification in casting. Middle carbon steel has the serious problem owing to the peritectic reaction of the $\delta\text{-}\gamma$ transformation that the non-uniform solidification shrinkage yields the longitudinal cracking on the steel surface. It has been revealed that the decrease in heat transfer leads to the spatially-uniform heat extraction from the shell, and as a consequence prevents the surface longitudinal cracking [1, 2]. The mould flux forms a slag film between the steel shell and the mould, which consists of liquid and solid (crystalline or crystalline + glassy) slag layers. The microstructures of the crystalline slag layers are columnar (or dendritic) and/or cubic [3]. The heat flux from the steel shell to the mould is composed of the conduction and radiation heat flows through the various slag layers, and the thermal resistance at the mould/slag interface [4]. It is known that in practice, the reduction in heat transfer is being made by forming crystals of cuspidine ($3CaO \cdot 2SiO_2 \cdot CaF_2$) in the flux film. [5]

Although many researchers have studied the mechanism by which crystallization reduces the heat flux across the mould flux layer, there has been no consensus obtained on the mechanism [6, 19]. In order to elucidate the mechanism, the authors have calculated the total heat flux on the basis of a heat transfer model involving conduction and radiation processes, with variation in parameters such as physical properties of mould flux, and have found that the reflectivity of the crystalline slag layer is an efficient factor for further reducing the heat transfer: [6] The reflectivity can be increased by crystallization of mold flux due to enhanced scattering of light by introduction of crystal grain boundaries. The radiation is reflected at the interface between the liquid and the crystalline slag layers and at the crystal grain boundaries. Increased reflectivity by crystallization causes more radiation energy to return from the crystalline slag layer to the steel shell, resulting in the reduction in the total heat flux across the flux film, leading to mild cooling. The reflectivity by crystallization may be affected by the microstructure of the crystalline slag layer and/or the degree of crystallization. Nakada has reported that the reflectivity of the crystalline slag layer is more widely changed by varying the crystal grain size rather than the degree of crystallization [20]. However, to the best of our knowledge, there is no investigation with regard to the effect of the crystalline morphology on the heat flux across the flux film. The aim of this study is to experimentally obtain the relationship between the microstructure of the crystalline slag layer and the heat transfer through the mould flux film.

METHODOLOGY

Sample Preparation

Table 1 shows the chemical compositions of five samples (Flux I-V). The samples were prepared from reagent grade SiO_2, CaF_2, NaF and $CaCO_3$ powders, the last being decomposed to CaO by heating at 1373 K for 36 ks in air. The reagents were weighted to the desired compositions and mixed in an alumina mortar. About 10 g of the mixtures were uniaxially pressed to make a pellet.

Table 1: Chemical compositions (mass%) of Flaxes I-V and the flow rates of the cooling water

	SiO_2	CaF_2	CaO	NaF	flow rate / ml/min
Flux I	36.23	22.73	31.05	10.00	180
Flux II	36.23	22.73	31.05	10.00	180
Flux III	36.23	22.73	31.05	10.00	180
Flux IV	36.23	22.73	31.05	10.00	160
Flux V	34.58	7.909	43.97	13.55	3000

Measurement

Figure 1 shows the schematic diagram of the experimental apparatus. A pellet sample was placed on a platinum plate (ca. 40 mm diameter and ca. 10 mm height), the rear surface of which a R-type thermocouple was attached to by spot welding. The sample was heated up to 1703 K at the rate of 8 $K \cdot min^{-1}$. After confirming that the sample was melted, the water-cooled copper block (36 mm diameter and 40 mm height) was placed onto the sample and held for ca. 5 min. The flow rates of the cooling water are given in Table 1. Subsequently, the sample together with the copper block and the platinum plate was quenched into water. The copper block and the platinum plate in this experiment correspond to the mould and the steel shell in the continuous casting, respectively. During the course of the experiments, the temperatures of the copper block, the platinum plate and the cooling water inlet and outlet for the copper block were monitored: the temperatures of the copper block were measured at 4.5 mm (T_1) and 19.5 mm (T_2) above the sample /copper block interface by K-type thermocouples. The temperature of the platinum plate (T_3) was measured at the rear surface by R-type thermocouple as described above, and the temperatures of the cooling water inlet and outlet (T_4 and T_5, respectively) were measured by T-type thermocouples.

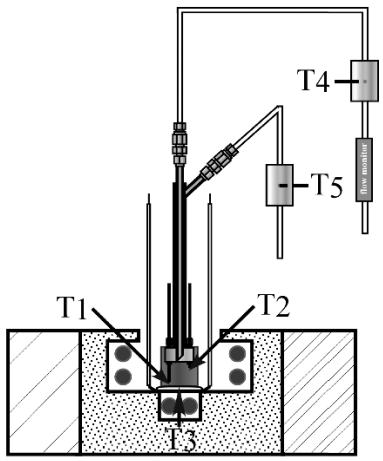

Figure 1: Schematic diagram of the experimental apparatus

The steady state heat flux across the flux film was calculated using the following Equations 1 and 2 assuming that the heat flows only vertically across the sample and the copper block.

$$q_{Cu} = \frac{\lambda_{Cu}}{1.5\times10^{-3}}(T_1 - T_2) \quad (1)$$

$$q_{water} = \frac{mC_p(T_5 - T_4)}{18^2\pi\times10^{-6}} \quad (2)$$

where q_{Cu} and q_{water} are the heat fluxes across the flux film calculated by Equations 1 and 2, respectively, λ_{Cu} is the thermal conductivity of copper (390 $W \cdot m^{-1} \cdot K^{-1}$), C_p is the specific heat at constant pressure of water (75.348 $J \cdot mol^{-1} \cdot K^{-1}$), and m is the flow rate of the cooling water (mol/sec). After the experiment, the phases of the samples were identified by x-ray diffraction analysis, and the cross sectional view of the sample was observed by electron probe micro analyzer (EPMA).

RESULTS

Figure 2 shows the temperature changes of the copper block (T_1 and T_2), the cooling water (T_4 and T_5) and the platinum plate (T_3) versus time from when the copper block was placed onto the sample until when the sample together with the copper block and the platinum plate was quenched into water for Flux IV. The heat flux across the sample attained the steady state ca. 100 s after the copper block was placed onto the sample. The heat flux across the sample was calculated by substitution of the average temperatures of T_1, T_2, T_4 and T_5 in the steady state into Equations 1 and 2. The obtained heat fluxes are tabulated in Table 2. It is found that the values of q_{water} are larger than those of q_{Cu} for all samples, which indicates that the horizontal heat flux from the four rod-like heating elements beside the copper block is not negligible although the heat insulating material is wound around the copper block. The value of q_{water} is more seriously affected by the horizontal heat flux than the value of q_{Cu} since the measurement points of T_4 and T_5 are farther from the sample than those of T_1 and T_2. The discrepancy between the values of q_{Cu} and q_{water} will be discussed in the next section.

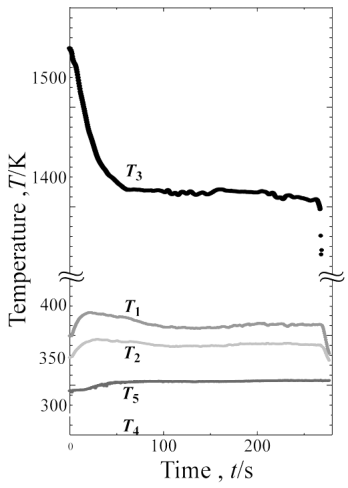

Figure 2: Shows the temperature changes of the copper block (T_1 and T_2), the cooling water (T_4 and T_5) and the platinum plate (T_3) versus time

Table 2 Heat fluxes, q_{Cu}, q_{water} and q_{true} ($x10^5$ W/m^2) for Fluxes I-V

	q_{cu}	q_{water}	q_{true}
Flux I	5.91	6.98	2.19
Flux II	5.56	5.91	1.83
Flux III	5.84	6.42	2.12
Flux IV	5.03	7.11	1.30
Flux V	4.09	6.11	0.351

Figures 3 and 4 show the BSE images of the cross sections of Flux III and Flux V. The upper and lower limits correspond to the contact faces with the copper block and the platinum plate, respectively. The cracks in the upper and lower sides were formed when the flux film was taken off the copper block and the platinum plate, respectively. It can be seen from Figures 3 and 4 that the flux films of Flux III and Flux V are composed of three layers; cubic crystals, smaller dendritic crystals growing in the random directions and larger dendritic crystals growing in the perpendicular direction to the contact faces with the platinum plate. It has been found that the flux films of other samples have the similar microstructures to those of Flux III and Flux V. The x-ray diffraction analyses reveal that the crystals in all flux films are cuspidine. It has been considered that the layer with larger dendritic crystals was the liquid slag layer: The layer was molten even after the copper block was placed onto the sample. Subsequently, the crystals have grown from the contact faces with the platinum plate under the abrupt temperature gradient while the sample was immersed in water. Hereafter, the three layers with cubic, smaller dendritic and larger dendritic cystals are denoted by the cubic-crystal, dendrite and slag layers, respectively.

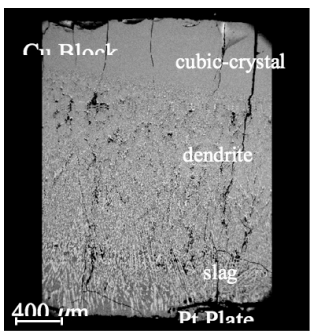

Figure 3: BSE images of the cross section of Flux III

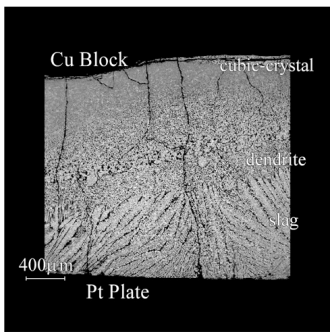

Figure 4: BSE images of the cross section of Flux V

The thicknesses of three layers were measured for five samples using the BSE images of the cross sections. The thickness of the layer was measured at 8-13 points for each layer of each sample. Table 3 summarizes the average thicknesses of the crystalline layer (summation of the thicknesses of the cubic-crystal and dendrite layers), the cubic-crystal, dendrite and slag layers.

Table 3: Average thicknesses of the crystalline layer (summation of the thicknesses of the cubic-crystal and dendrite layers), the cubic-crystal, dendrite and slag layers (mm) for Fluxes I-V

	Crystalline layer	cubic-crystal layer	dendrite layer	slag layer
	error	error	error	error
Flux I	2.27 0.361	0.544 0.167	1.73 0.320	0.132 0.048
Flux II	2.52 0.243	0.170 0.219	2.35 0.105	0.354 0.138
Flux III	2.34 0.220	0.581 0.160	1.76 0.150	0.308 0.116
Flux IV	2.35 0.536	0.425 0.407	1.76 0.150	0.521 0.112
Flux V	1.05 0.346	0.536 0.256	0.517 0.232	0.588 0.401

DISCUSSION

True Heat Flux across the Flux Film

As described in the last section, the discrepancy between the values of q_{Cu} and q_{water} is attributed to the horizontal heat flux from the heating elements beside the copper block. The temperature distribution in the copper block has been calculated based on the simple model: (i) The copper block is rectangular (two lengths of sides are $2B$ and W). (ii) The temperature T is a function of z alone, which is the vertical direction. (iii) The radiation energy is exposed on both sides with the side length of W, and the radiation heat flux is given by $q = h\,(T_a - T)$, in which h is constant, T_a is the temperature of heating elements. A thermal energy balance on a segment between two plates $z = z$ and $z = z + \Delta z$ gives:

$$q_z(z) \cdot 2BW - q_z(z + \Delta z) \cdot 2BW - h(2W\Delta z)(T - T_a) = 0 \tag{3}$$

Division by $2BW\Delta z$ and taking the limit as Δz approaches zero gives

$$-\frac{dq_z}{dz} = \frac{h}{B}(T - T_a) \tag{4}$$

Insertion of Fourier's law ($q_z = -\lambda_{Cu} \cdot dT/dz$) gives

$$\frac{d^2T}{dz^2} = \frac{h}{\lambda_{Cu}B}(T - T_a) \tag{5}$$

This equation is to be solved with the boundary conditions: (1) at $z = z_1$, $T = T_1$, (2) at $z = z_2$, $T = T_2$. The following dimensionless quantities are introduced.

$$N = (z_2 - z_1)\sqrt{\frac{h}{\lambda B}} \tag{6}$$

$$\xi = \frac{z - z_1}{z_2 - z_1} \tag{7}$$

Then, we get the equation of temperature distribution.

$$T = T_a + \frac{T_2 - T_a - e^{-N} \cdot (T_1 - T_a)}{e^N - e^{-N}} \cdot e^{N\xi} + \frac{-(T_2 - T_a) + e^N (T_1 - T_a)}{e^N - e^{-N}} \cdot e^{-N\xi} \quad (8)$$

True heat flux across the flux film q_{true} has been obtained by the following equation.

$$q_{true} = -\lambda_{Cu} \left(\frac{dT}{dz} \right)_{z=0} \quad (9)$$

The constant h has been calculated by the following:

$$h \left(T_a - \frac{T_1 + T_2}{2} \right) = \sigma \left({T_a}^4 - \left(\frac{T_1 + T_2}{2} \right)^4 \right) \quad (10)$$

where σ is the Stefan-Boltzmann constant. Substitution of $2B = W = 16$ mm, $T_a = 1703$ K, $z_1 = 4.5$ mm and $z_2 = 19.5$ mm into Equations 6 -10 gives the true heat fluxes q_{true}, which are included in Table 2.

Relationship between the Heat Flux across the Flux Film and the Thicknesses of the Crystalline, Cubic-crystal, Dendrite and Slag Layers

Figures 5(a-d) show the true heat flux across the flux film as a function of the thicknesses of crystalline (a) cubic-crystal (b) dendrite (c) and slag layers (d). If the heat flux is dependent on the thicknesses of crystalline, cubic-crystal and dendrite layers, the heat flux should decrease with an increase in these thicknesses since the radiation is more reflected at the crystal grain boundaries while transmitting through the sample. In fact, the dependencies of the heat fluxes on the thicknesses are not the case. Consequently, it is considered that the heat flux is independent of the thicknesses of the crystalline, cubic-crystal and dendrite layers, which indicates that the reflection of radiation at the crystal grain boundaries does not affect the total heat flux across the sample. On the other hand, the inspection of Figure 5(d) demonstrates that there may be a negative dependency of the heat flux on the thickness of slag layer although the uncertainty in the slag-layer thickness is very large. This suggests the possibility that the heat flux is most dominantly affected by the conduction heat flux across the slag layer. In fact, the heat flux, which is estimated assuming that the thermal conductivity of the slag layer is 0.26 $W \cdot m^{-1} \cdot K^{-1}$ [5] and the temperature difference between two ends of the slag layer is 50 K, decreases much faster than the measured heat flux with an increase in the thickness of slag layer. As a result, it is considered that the heat flux is independent of the thickness of slag layer.

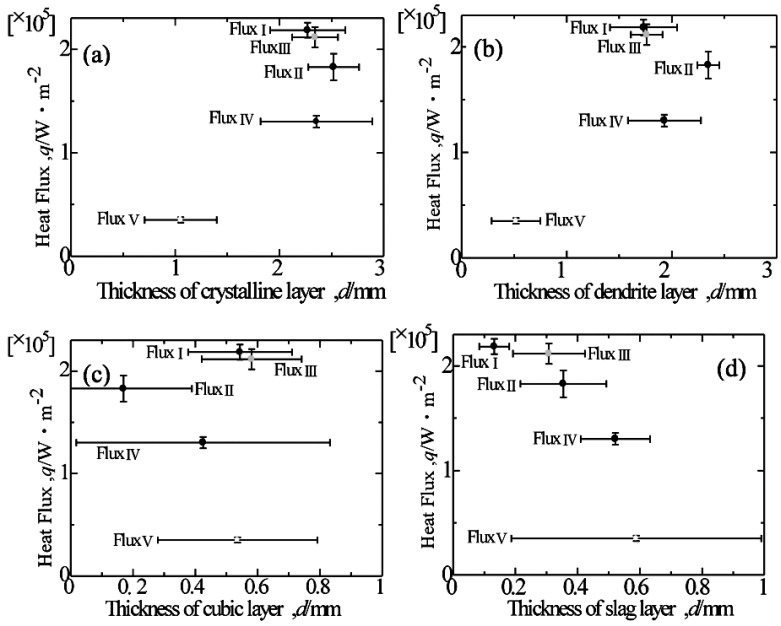

Figure 5: True heat flux across the flux film as a function of the thicknesses of crystalline (a), cubic-crystal (b), dendrite (c) and slag layers (d)

Relationship between the Heat Flux across the Flux Film and the Roughness of the Interface between the Slag and the Crystalline Layers

The conclusion that the reflection of radiation at the crystal grain boundaries does not affect the total heat flux across the flux film may imply that the increased reflectivity by crystallization leading to the reduction in the total heat flux could be mainly due to the increased reflection at the interface between the liquid and the crystalline slag layers. In order to investigate the possibility, the roughnesses of the interface between slag and crystalline layers, *i.e.*, the widths of the dendrite in the dendrite layer are compared among the samples. Figure 6 shows the BSE images of the cross sections of Flux III and Flux V around the interface between slag and crystalline layers. Fluxes I, II and IV have the similar crystalline morphology to that of Flux III. It is found that the widths of the dendrite in the dendrite layer of Flux I-IV and Flux V are 5-20 μm and 40-80 μm, respectively. According to the Wien's displacement law, the wavelength with the maximum in the Planck distribution at the temperature at the interface between the liquid and the crystalline slag layers, *i.e.*, the liquidus temperature of the slag, is ca. 2 μm. Since the wavelength of the radiation is in the same order as the width of the dendrite at the interface, the scattering of light should be considered based on the Mie formulae [21]. The cross sections for extinction by a homogeneous sphere monotonically increases with an increase in the value of $4\pi a(m-1) / \lambda$ when the value is less than ca. 4.5, where $2a$ is the diameter of the sphere, m is the ratio of the refractive index of the sphere to that of the matrix, and λ is the radiation wavelength. The Mie effect is applied to the present study. The refractive indexes of the molten and crystalline slags are 1.55-1.58 and 1.59, respectively [6]. Therefore, it can be considered by calculation that the cross sections for extinction monotonically increases with increasing the diameter of the scattering particles $2a$ when $2a$ is less than 30-110 μm. If assuming that the width of the dendrite at the interface can be regarded as the diameter of the scattering particles $2a$, it is considered that the reflection of radiation increases, that is, the total heat flux across the flux film reduces with an

increase in the width of the dendrite at the interface. This is in accord with the present result that the heat flux of Flux V is extremely small compared to those of the other fluxes, which implies that the reflection of radiation at the interface between the liquid and the crystalline slag layers is a dominant factor for reducing the heat flux across the flux film.

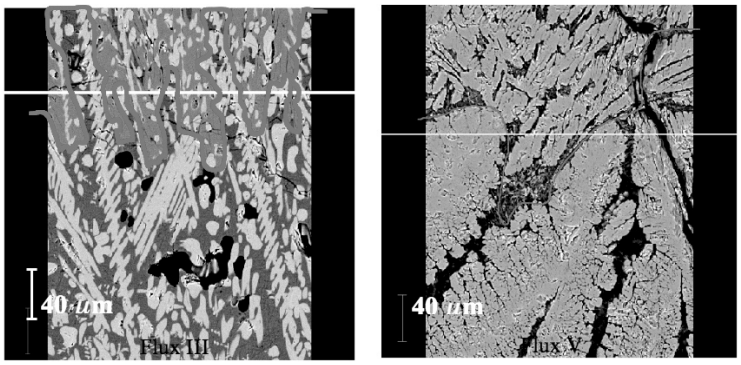

Figure 6: BSE images of the cross sections of Flux III and Flux V around the interface between slag and crystalline layers

CONCLUSIONS

Our previous research has revealed that the reflectivity of the crystalline slag layer is an efficient factor for further reducing the heat flux across the flux film. The radiation is reflected at the interface between the liquid (slag) and the crystalline layers and/or at the crystal grain boundaries. In order to investigate the effect of the crystalline morphology of the crystalline slag layer on the heat flux across the flux film, the heat flux has been measured so as to elucidate the dependencies of the heat flux on the thicknesses of the slag and the crystalline layers and the roughness of the interface between the slag and the crystalline layers.

- The heat flux is independent of the thicknesses of the crystalline, cubic-crystal, dendrite and slag layers, which indicates that the reflection of radiation at the crystal grain boundaries does not affect the total heat flux across the sample.
- The flux film having the larger width of the dendrite at the interface between the slag and the crystalline layers exhibits the smaller heat flux, which can be explained by the Mie effect. This result implies that the reflection of radiation at the interface between the liquid and the crystalline slag layers is a dominant factor for reducing the heat flux across the flux film.

REFERENCES

Sugitani, Y., Nakamura, M. & Watanabe, T. (1981). *Tetsu-to-Hagané*. 67, 102. [1]

Billany, T. J. H., Normanton, A. S. & Grieveson, P. (1991). *Ironmaking Steelmaking*. 18, No. 6, p. 403. [2]

Nakada, H. & Nagata, K. (2006). ISIJ Int., 46, 441. [3]

Mills, K. C. & Fox, A. B. (2003). ISIJ Int., 43, 1479. [4]

Hanao, M., Kawamoto, M. & Watanabe, T. (2004). ISIJ Int., 44, 827. [5]

Nakada, H., Susa, M., Seko, Y., Hayashi, M. & Nagata, K. (2008). ISIJ Int., 48, 446. [6]

Taylor, R. & Mills, K. C. (1988). *Ironmaking Steelmaking*. 15, 187. [7]

Bagha, S., Machingawuta, N. C. & Grieveson, P. (1988). Proc. of the 3rd Int. Conf. on Molten Slags and Fluxes, The Institute of Metals, London, U.K., 235. [8]

Susa, M., Nagata, K. & Mills, K. C. (1993). *Ironmaking Steelmaking*. 20, 372. [9]

Yamauchi, A., Sorimachi, K., Sakuraya, T. & Fujii, T. (1993). ISIJ Int., 33, 140. [10]

Susa, M., Mills, K. C., Richardson, M. J., Taylor, R. & Stewart, D. (1994). *Ironmaking Steelmaking*. 21, 279. [11]

Shibata, H., Emi, T., Waseda, Y., Kondo, K., Ohta, H. & Nakajima, K. (1996). *Tetsu-to-Hagané*. 82, 46. [12]

Kawamoto, M., Tsukaguchi, Y., Nishida, N., Kanazawa, T. & Hiraki, S. (1997). ISIJ Int., 37, 134. [13]

Watanabe, K., Suzuki, M., Murakami, K., Kondo, H., Miyamoto, A. & Shiomi, T. (1997). *Tetsu-to-Hagané*. 83, 31. [14]

Cho, J. W., Shibata, H., Emi, T. & Suzuki, M. (1998). ISIJ Int., 38, 268. [15]

Cho, J. W., Shibata, H., Emi, T. & Suzuki, M. (1998). ISIJ Int., 38, 440. [16]

Cho, J. W., Emi, T., Shibata, H. & Suzuki, M. (1998). ISIJ Int., 38, 834. [17]

Tsutsumi, K., Nagasaka, T. & Hino, M. (1999). ISIJ Int., 39, 1150. [18]

Hanao, M. & Kawamoto, M. (2006). *Tetsu-to-Hagané*. 92, 655. [19]

Nakada, H. (2007). PhD thesis, Tokyo Institute of Technology. [20]

Van de Hulst, H. C. (1957). *Light Scattering by Small Particles*. John Wiley & Sons, Inc. U.S.A., Chap. 19. [21]